Supporting Information

Electrocatalytic Water Oxidation at Amorphous Trimetallic Oxides

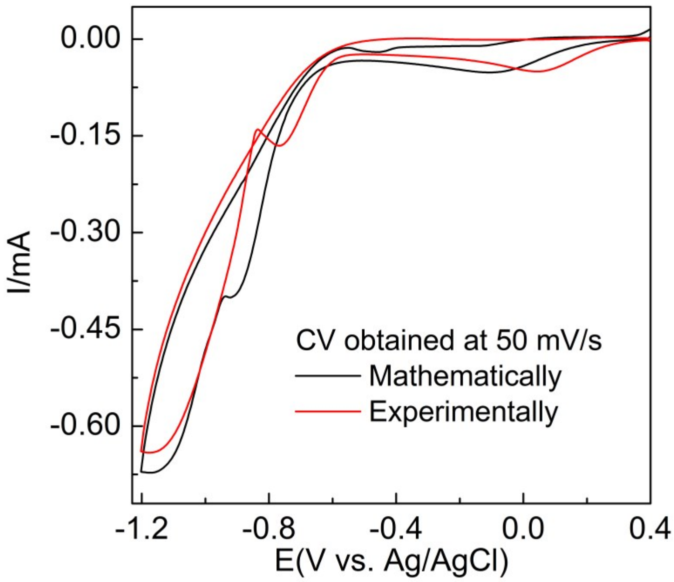

Figure S1 Comparison between cyclic voltammograms obtained at 50 mV s^{-1} at an Au electrode for the deposition of FeCoNiOx and the mathematical summation of the individual CVs recorded in Figure 1 of the main manuscript.

Nucleation-Growth Mechanism study:

For the deposition of FeCoNiOx, chronamperometry was used which can be used to determine the nucleation growth mechanism via use of the Hills-Scharifker method.[1] This theory describes two limiting cases, i.e. progressive and instantaneous growth mechanisms, for the initial stages of 3D nucleation and 2D growth of deposited nuclei. These processes can be described by the following

$$\left(\frac{I}{I_m}\right)^2 = \frac{1.2254}{t/t_m}\left\{1-\exp\left[-2.3367\left(\frac{t}{t_m}\right)^2\right]\right\}^2 \quad (1)$$

which represents 3D progressive nucleation and 2D growth and

$$\left(\frac{I}{I_m}\right)^2 = \frac{1.9542}{t/t_m}\left\{1-\exp\left[-1.2564\left(\frac{t}{t_m}\right)\right]\right\}^2 \quad (2)$$

which represents 3D instantaneous and 2D growth Where, I = current at time t and I_m = maximum current density at time $t_{m.}$

After plotting the experimental data in the dimensionless form via a plot of $(I/I_m)^2$ versus (t/t_m) it was observed that the best fit is achieved at early times (< 3 s) for the instantaneous nucleation of $FeCoNiO_{x(s)}$ on the electrode surface. After 3 s the data deviates from the theoretical curve which is consistent with the SEM image of the sample which shows significant outward growth. The Hills-Scharifker model assumes the deposition of hemispherical nuclei which grow in a uniform manner which is not the case here.

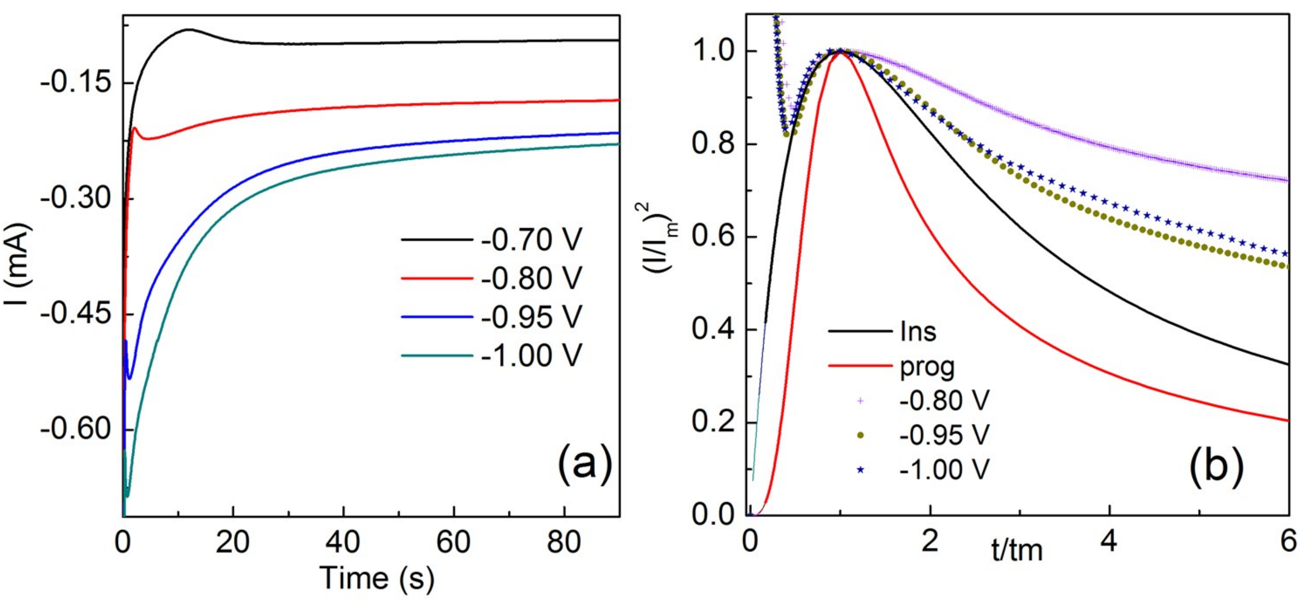

Figure S2: (a) current-time curves obtained at different applied potentials and (b) non-dimensional plots of (I/Im)2 vs. t/tm for the electrodeposition of $CoNiFeO_xH_y$. Overlaid are the theoretical curves calculated using eqn (1) and (2) for progressive ( ) and instantaneous ( ) nucleation and diffusion limited growth.

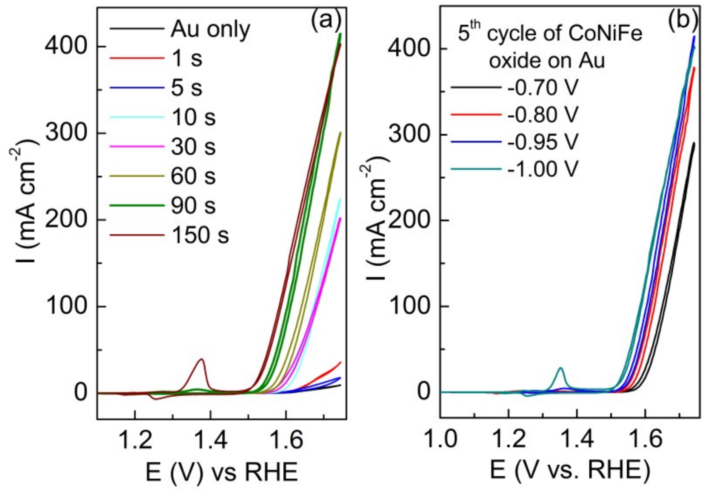

Figure S3. OER performance for $CoNiFeO_x$ electrodeposited form 8 mM of $Co(NO_3)_2.6H_2O$, $N_2NiO_6.6H_2O$ and $Fe(NO_3)_3.9H_2O$ solution mixture on (a) Au substrate electrodeposited at -0.95 V at different deposition time and (b) at different applied potential for 90 s (fifth cycle is shown). Cyclic voltammograms were recorded at 10 mV s^{-1} in 0.10 M NaOH.

Although CoNiFeOx@Au electrodeposited for 150 s resulted in similar OER performance and a slightly better onset potential on the voltametric timescale, the catalyst deactivated more readily compared to the sample deposited for 90 s and therefore this time was chosen as our optimum deposition potential. In addition the sample electrodeposited at -0.95 V also showed the better long term stability and hence was chosen as the optimal time.

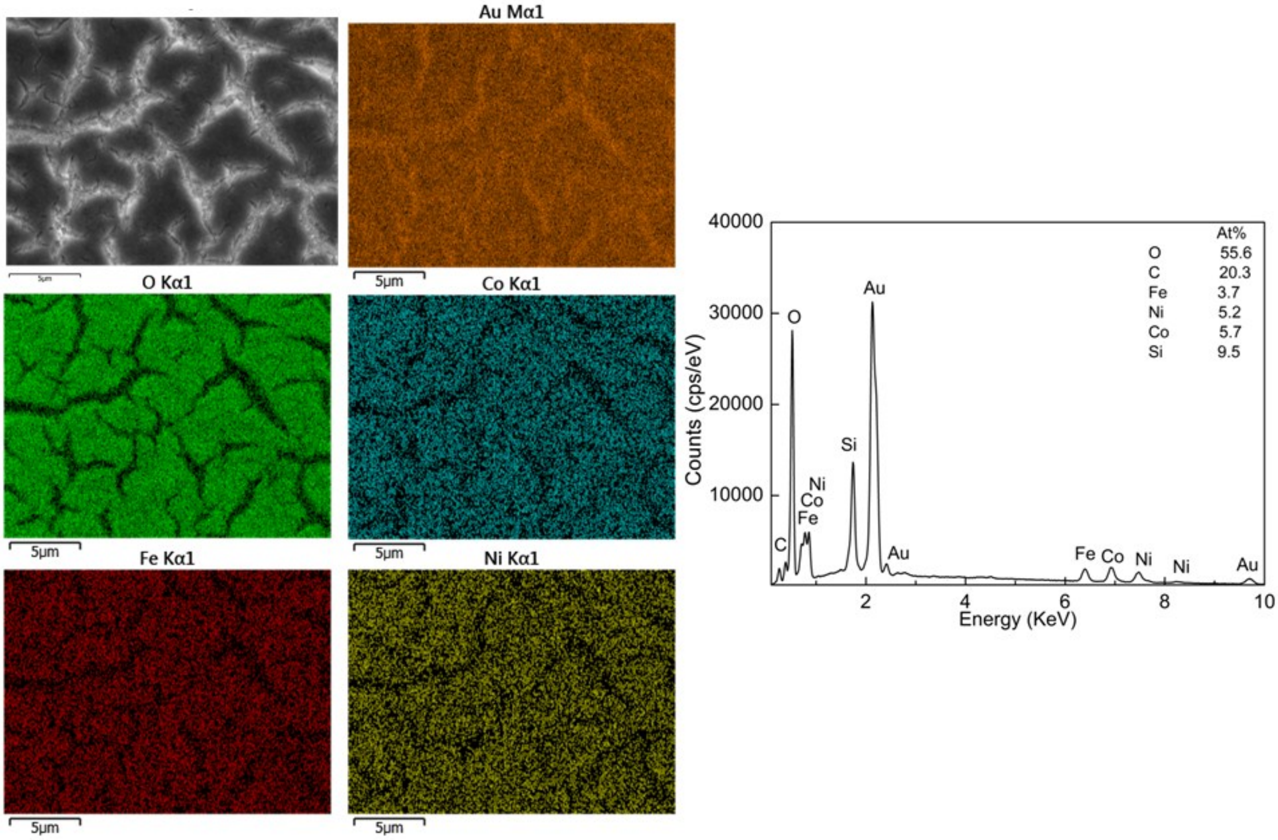

Figure S4. EDX-SEM mapping for mixed hydroxide/AU after deposition.

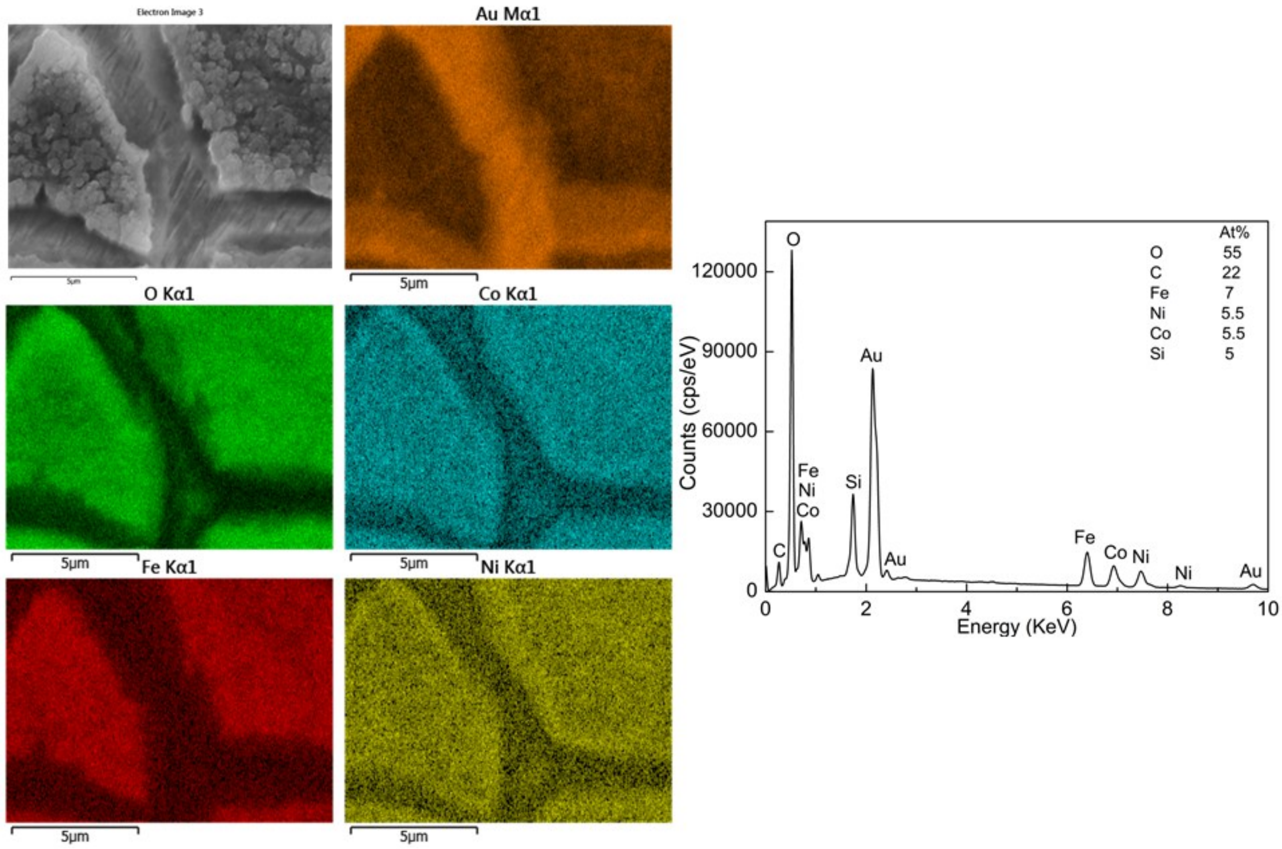

Figure S5. EDX-SEM mapping for mixed hydroxide/AU after 5 cycles in the OER region.

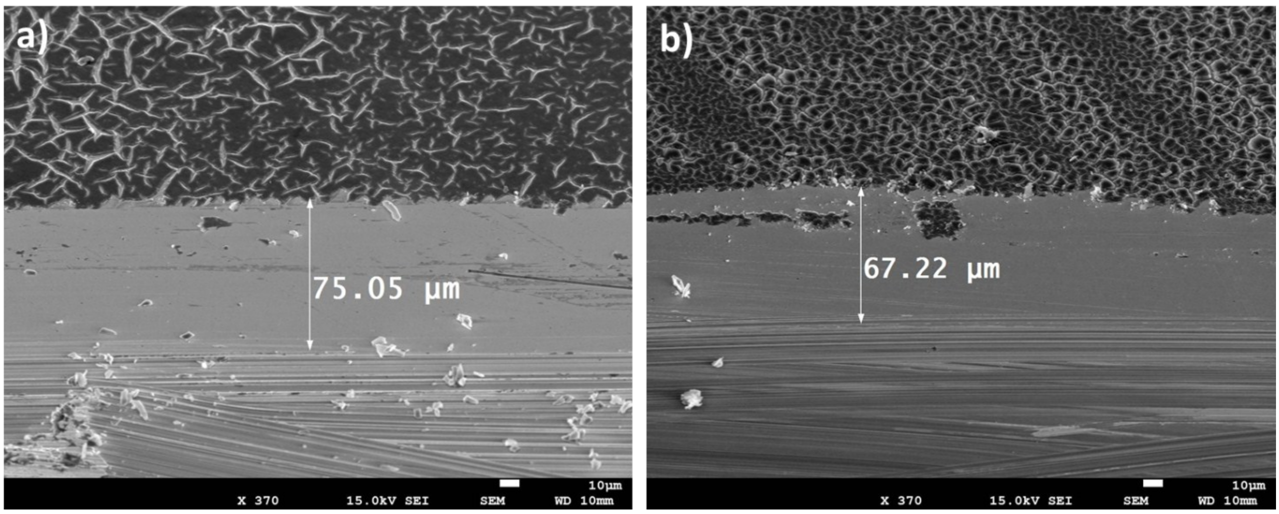

Figure S6: Side profile SEM images of $CoNiFeO_xH_y$ electrodeposited film on an Au electrode for 90 sec at -0.95 V before (a) and after (b) the OER.

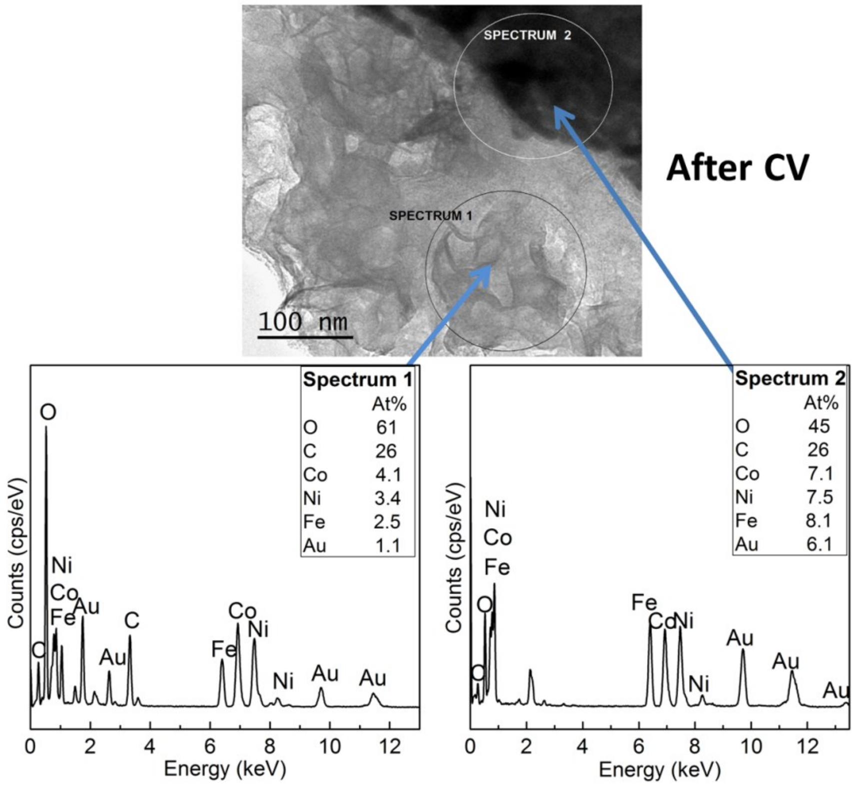

Figure S7: EDS-TEM spectra of different sites of mixed oxide electrodeposited onto a Au TEM grid post OER.

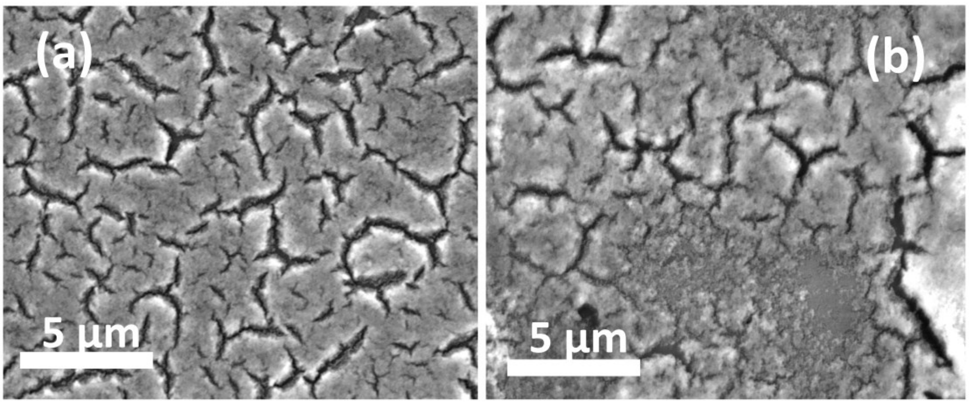

Figure S8. SEM images of $CoNiFeO_xH_y$ electrodeposited film on GC electrode for 90 sec at -0.95 V.

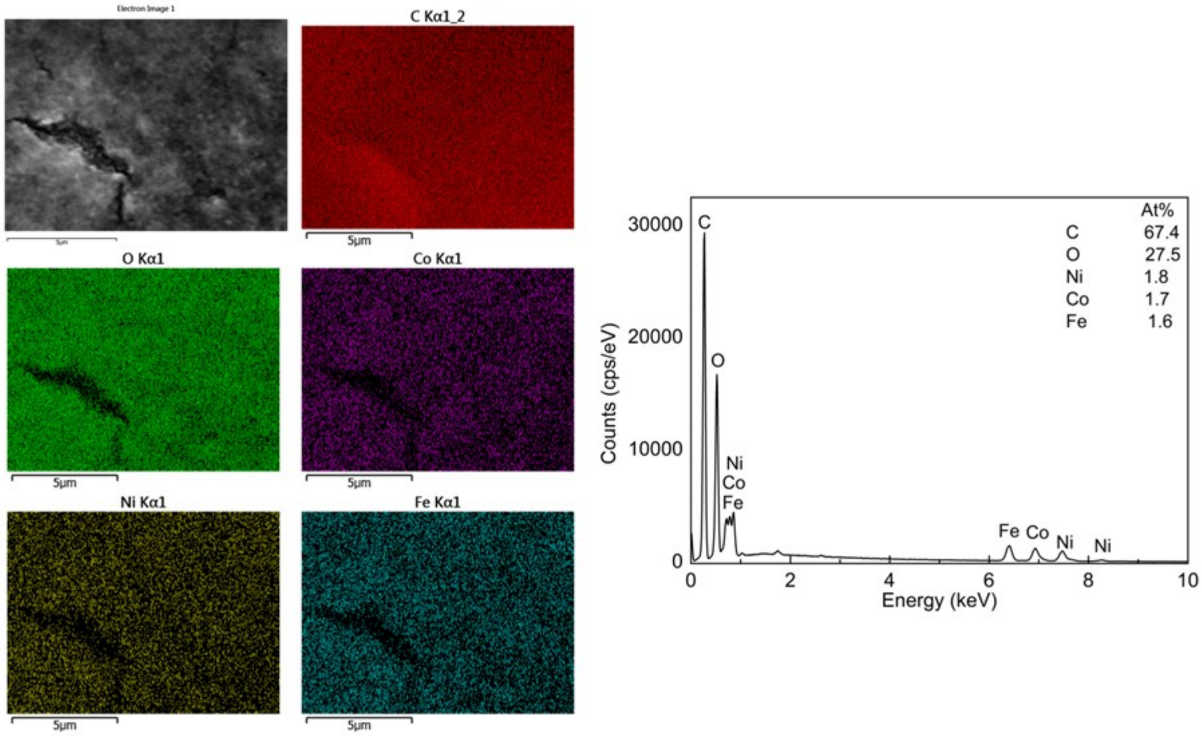

Figure S9. EDX-SEM mapping for mixed hydroxide/GC after 5 cycles in the OER region.

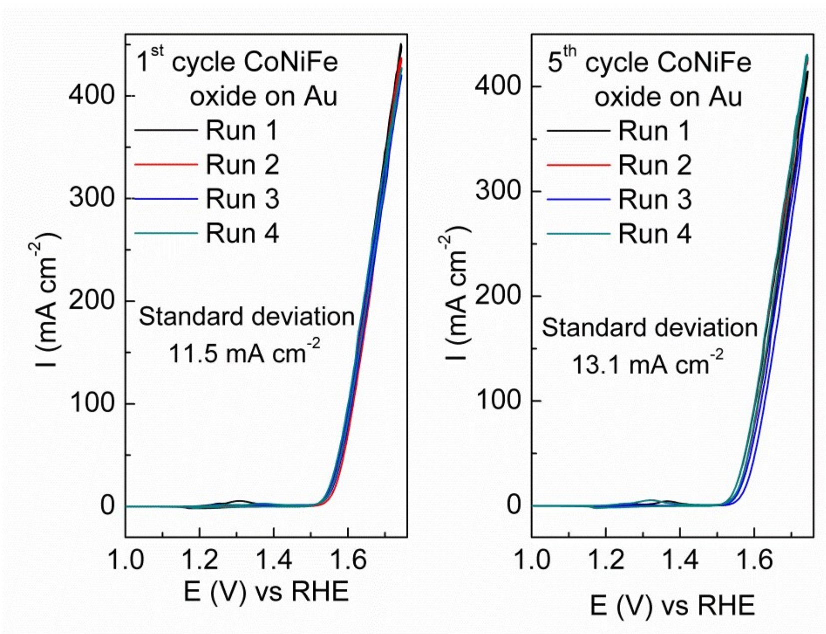

Figure S10: OER performance for $CoNiFeO_x$ electrodeposited form 8 mM of $Co(NO_3)_2.6H_2O$, $N_2NiO_6.6H_2O$ and $Fe(NO_3)_3.9H_2O$ solution mixture on an Au substrate electrodeposited at -0.95 V for 90 showing four separate samples. Standard deviation is quoted from measuring the current at 1.67 V.

Table S1:

Material	Overpotential (η) in mV at 10 mA cm^{-2}	Tafel slope (mV/dec)	TOF (s^{-1})	Reference
α-CoFeNiOx	310	≈32	2.1	This work
α-CoFeOx	300	≈41	2.01	This work
α-CoNiOx	300	≈43	0.67	This work
α-NiFeOx	280	≈40	2.00	This work
NiFe-LDH/CNT	308	35		[2]
Ni-CoOOH	280	36		[3]
$Ba_{0.5}Sr_{0.5}Co_{0.8}Fe_{0.2}O_{3-\delta}$	350	60		[4]
$BaCo_{0.9-x}Fe_xSn_{0.1}O_{3-\delta}$	430	69		[5]
NiCo@NCNTs	410	177		[6]
$LiCo_{0.8}Fe_{0.2}O_2$	340	50		[7]
N-Co_9S_8/Graphene	409	82.7		[8]
Ni_3S_2/AT-Ni foam	217	163		[9]
NG-NiCo	350	614		[10]
Porous Ni-Fe oxide	328		0.12	[11]
CoFe-CNFs	570			[12]
$a\mathrm{Fe}_{40}\mathrm{Ni}_{60}\mathrm{O}_x$		34		[13]
$a\mathrm{Fe}_{39}\mathrm{Co}_{39}\mathrm{Ni}_{22}\mathrm{O}_x$		40		[13]
Co/N-CNTs	390	67		[14]
CoO@N/S-CNF	320	95		[15]
S,N-Fe/N/C-CNT	370	82		[16]
$CoWO_4$ NFs	436	202		[17]
$Ni_{0.71}Fe_{0.29}(OH)_x$	296	58	0.0146	[18]
Co_3O_4/N-graphene	360	67	0.0031	[19]
Amorphous $CoFe_2O_{3.66}$ Crystalline $CoFe_2O_4$	490 56	48 61		[20]
a-$\mathrm{FeCoNiO}_x$		31		[21]
$FeCoNiO_x$		37		[22]
$FeNi_8Co_2$ LDH	220	42	0.7	[23]
$NiFeO_x$/C	300		0.45	[24]
Amorphous $Ni(OH)_2$	344	46		[25]

1. B. Scharifker and G. Hills, *Electrochimica Acta*, 1983, **28**, 879-889.
2. M. Gong, Y. Li, H. Wang, Y. Liang, J. Z. Wu, J. Zhou, J. Wang, T. Regier, F. Wei and H. Dai, *Journal of the American Chemical Society*, 2013, **135**, 8452-8455.
3. Z. Chen, C. X. Kronawitter, Y.-W. Yeh, X. Yang, P. Zhao, N. Yao and B. E. Koel, *Journal of Materials Chemistry A*, 2017, **5**, 842-850.
4. J. Suntivich, K. J. May, H. A. Gasteiger, J. B. Goodenough and Y. Shao-Horn, *Science*, 2011, **334**, 1383-1385.
5. X. Xu, C. Su, W. Zhou, Y. Zhu, Y. Chen and Z. Shao, *Advanced Science*, 2016, **3**, n/a-n/a.
6. J. Yu, Y. Zhong, W. Zhou and Z. Shao, *Journal of Power Sources*, 2017, **338**, 26-33.
7. Y. Zhu, W. Zhou, Y. Chen, J. Yu, M. Liu and Z. Shao, *Advanced Materials*, 2015, **27**, 7150-7155.
8. S. Dou, L. Tao, J. Huo, S. Wang and L. Dai, *Energy & Environmental Science*, 2016, **9**, 1320-1326.

9. C. Ouyang, X. Wang, C. Wang, X. Zhang, J. Wu, Z. Ma, S. Dou and S. Wang, *Electrochimica Acta*, 2015, **174**, 297-301.
10. S. Chen, J. Duan, M. Jaroniec and S. Z. Qiao, *Angewandte Chemie International Edition*, 2013, **52**, 13567-13570.
11. J. Qi, W. Zhang, R. Xiang, K. Liu, H.-Y. Wang, M. Chen, Y. Han and R. Cao, *Advanced Science*, 2015, **2**, n/a-n/a.
12. B. Jeong, D. Shin, J. K. Lee, D. H. Kim, Y. D. Kim and J. Lee, *Physical Chemistry Chemical Physics*, 2014, **16**, 13807-13813.
13. R. D. L. Smith, M. S. Prévot, R. D. Fagan, S. Trudel and C. P. Berlinguette, *Journal of the American Chemical Society*, 2013, **135**, 11580-11586.
14. Y. Liu, H. Jiang, Y. Zhu, X. Yang and C. Li, *Journal of Materials Chemistry A*, 2016, **4**, 1694-1701.
15. T. Liu, Y.-F. Guo, Y.-M. Yan, F. Wang, C. Deng, D. Rooney and K.-N. Sun, *Carbon*, 2016, **106**, 84-92.
16. P. Chen, T. Zhou, L. Xing, K. Xu, Y. Tong, H. Xie, L. Zhang, W. Yan, W. Chu, C. Wu and Y. Xie, *Angewandte Chemie International Edition*, 2017, **56**, 610-614.
17. T. Tian, J. Jiang and L. Ai, *Electrochimica Acta*, 2017, **224**, 551-560.
18. Y. Q. Gao, X. Y. Liu and G. W. Yang, *Nanoscale*, 2016, **8**, 5015-5023.
19. Y. Liang, Y. Li, H. Wang, J. Zhou, J. Wang, T. Regier and H. Dai, *Nat Mater*, 2011, **10**, 780-786.
20. A. Indra, P. W. Menezes, N. R. Sahraie, A. Bergmann, C. Das, M. Tallarida, D. Schmeißer, P. Strasser and M. Driess, *Journal of the American Chemical Society*, 2014, **136**, 17530-17536.
21. R. D. L. Smith, M. S. Prévot, R. D. Fagan, Z. Zhang, P. A. Sedach, M. K. J. Siu, S. Trudel and C. P. Berlinguette, *Science*, 2013, **340**, 60-63.
22. J. Fan, Z. Chen, H. Shi and G. Zhao, *Chemical Communications*, 2016, **52**, 4290-4293.
23. X. Long, S. Xiao, Z. Wang, X. Zheng and S. Yang, *Chemical Communications*, 2015, **51**, 1120-1123.
24. M. Görlin, M. Gliech, J. F. de Araújo, S. Dresp, A. Bergmann and P. Strasser, *Catalysis Today*, 2016, **262**, 65-73.
25. Y. Gao, H. Li and G. Yang, *Crystal Growth & Design*, 2015, **15**, 4475-4483.